Journal of Power Sources 270 (2014) 42–52

Contents lists available at ScienceDirect

Journal of Power Sources

journal homepage: www.elsevier.com/locate/jpowsour

Synthesis of hierarchical TiO_2 flower-rod and application in CdSe/CdS co-sensitized solar cell

Libo Yu, Zhen Li, Yingbo Liu, Fa Cheng, Shuqing Sun*

Department of Chemistry, Tianjin University, Tianjin 300072, PR China

HIGHLIGHTS

- Double-layered TiO_2 flower-rod structure was directly grown on FTO glass.
- A possible formation mechanism of this TiO_2 flower-rod architecture was proposed.
- This TiO_2 architecture was used in CdSe/CdS co-sensitized solar cell.
- The efficiency was significantly enhanced with CdSe/CdS/TiO_2 flower-rod electrode.

ARTICLE INFO

Article history:
Received 12 May 2014
Received in revised form
9 July 2014
Accepted 15 July 2014
Available online 24 July 2014

Keywords:
Titanium dioxide flower-rod
Hydrothermal method
Cadmium sulfide
Cadmium selenide
Quantum dots sensitized solar cell

ABSTRACT

A hierarchical double-layered TiO_2 flower-rod structure composed of three-dimensional (3D) TiO_2 flowers and one-dimensional (1D) nanorods on transparent fluorine-doped tin oxide (FTO) conducting glass has been synthesized by a facile hydrothermal method. The possible formation mechanism of the hierarchical architecture is also proposed. When used in CdSe/CdS quantum dots co-sensitized solar cells (QDSSCs), the 1D ordered rutile nanorods at bottom can accelerate the electron transfer rate by providing direct electrical pathway for photogenerated electrons, while the 3D flowers formed on the top of nanorods can increase the adsorption of QDs due to the enlarged areas, and can also be used as a scattering layer. The performance of the CdSe/CdS/TiO_2 flower-rod solar cell can achieve a short-circuit current density (J_{sc}) of 13.46 mA cm^{-2}, and a open-circuit voltage (V_{oc}) of 0.42 V, with a maximum power conversion efficiency of 2.31% under one sun illumination (AM 1.5 G, 100 mW cm^{-2}), which is greatly higher than that of CdSe/CdS/TiO_2 nanorod solar cell (1.63%).

1. Introduction

Nanostructured titanium dioxide (TiO_2) is an important material which is widely applied in areas related to photoelectrolysis, photocatalysis, gas sensing, photovoltaic devices, etc [1–5]. Nanostructured TiO_2 was usually used as photoanode substrate for quantum dots sensitized solar cells (QDSSCs) because of its several advantages, such as suitable conduction band position, stable chemical and physical properties, and inexpensive cost [6,7]. Up to now, nanostructured TiO_2 with various morphologies has been synthesized, such as nanoparticles, nanorods, nanotubes, and so on [8–10]. Recently, several works have been done on the 3D structural TiO_2 which based on 1D rutile nanorod [11,12], but seldom researches have been reported on the formation of double-layered hierarchical TiO_2 nanostructures, which consisted of 1D rutile TiO_2 nanorods and 3D TiO_2 flowers. The photoelectrochemical properties of TiO_2, especially in sensitized-solar cells, can be improved with formation of double-layered TiO_2 structure. Previous research work reported by Ho et al. [13] have revealed that an enhanced performance of dye-sensitized solar cell can be obtained with double-layered metal-based flexible TiO_2 photoanode which consisted of TiO_2 nanotubes and TiO_2 nanoparticles as the underlayer and overlayer, respectively. In addition, our group has reported that free-standing TiO_2 nanowire/nanotube (NW/NT) structure applied in QDSSCs is also favorable for the enhancement of photovoltaic performance [14]. However, multiple steps are involved in the fabrication of this kind of free-standing TiO_2 NW/NT photoanode, which increases the complexity of the operation. Moreover, hierarchical TiO_2 flower-rod structure which prepared by one-step hydrothermal, recently reported by our group, as photoanode in Mn-doped CdS QDSSCs has an important effect on the improvement of solar cell performance [15]. Hence, the hierarchical TiO_2 flower-rod film on transparent FTO glass which prepared with easy

* Corresponding author. Tel.: +86 13920690912.
E-mail address: sunshuqing@tju.edu.cn (S. Sun).

http://dx.doi.org/10.1016/j.jpowsour.2014.07.091
0378-7753/

fabrication process may show potential value in CdSe/CdS co-sensitized solar cell. In QDSSCs based on hierarchical TiO_2 flower-rod architecture, 1D nanorods can offer direct electronic pathway, accelerating the electrons transfer rate and reducing recombination of electrons and holes [16–19]; meanwhile 3D TiO_2 flowers can provide the increased surface areas, leading to more adsorption of QDs and more light absorption. Furthermore, 3D TiO_2 flowers can also be used as a scattering layer to enhance the light harvesting and improve the performance of QDSSCs.

Various narrow-band-gap semiconductors quantum dots such as CdS, CdSe, PbS, PbSe and InP are commonly used as sensitizers in QDSSCs [20–23] due to their several attractive characteristics, such as the tunable band gap, high extinction coefficients, large intrinsic dipole moments, multiple excitons generation (MEG), and hot electron injection [24–26]. Among these semiconductor QDs, CdS and CdSe have been paid much attention due to their appropriate band gap of 2.25 eV and 1.70 eV in bulk, respectively, which can allow the extension of absorption band to the visible region and show better performance in light harvesting under visible region [27]. Comparing these two kinds of QDs, CdS has a higher conduction band edge with respect to TiO_2 [28], which is advantageous to the injection of excited electrons from conduction band of CdS, resulting in high charges separation efficiency. Nevertheless, the band gap of CdS (2.25 eV in bulk) determines its maximum absorption range can only reach to approximately 550 nm, which means that a small portion of visible light can be utilized to produce photoexcited electrons. On the contrary, expanding the absorption edge close to 730 nm can be obtained with CdSe, but with a lower electron injection efficiency than CdS due to its conduction band edge is located below the conduction band of TiO_2 [28]. To incorporate both the advantages of these two kinds of materials, CdS and CdSe were usually used as co-sensitizers. The co-sensitized structure of CdS and CdSe has been proved to be advantageous over single CdS or CdSe in QDSSCs [29]. Currently, three methods are commonly used in the deposition of QDs on TiO_2: (i) in situ growth of QDs by chemical bath deposition (CBD) or successive ionic layer adsorption and reaction (SILAR) [30], (ii) assemble of presynthesized colloidal QDs with linker molecules [31], (iii) deposition of QDs by electrochemical atomic layer deposition (EC-ALD) method [32,33]. Among these methods, the CBD is the most widely used method due to the direct contact, high coverage of QDs on TiO_2 surface, and facile preparation process. Therefore, the CBD approach has been adopted to sensitize CdSe/CdS QDs on TiO_2 film in this work.

In this study, a hierarchical double-layered TiO_2 flower-rod structure film on FTO glass was successfully fabricated by a facile hydrothermal method and was decorated with coupled QDs (CdS and CdSe) through in situ chemical bath deposition (CBD) to form a photoanode which can be directly illuminated in QDSSCs. The CdSe/CdS/TiO_2 flower-rod solar cell exhibited much better performance than the QDSSCs based on CdSe/CdS/TiO_2 nanorod, CdS/TiO_2 flower-rod, and CdSe/TiO_2 flower-rod photoanodes. This kind of CdSe/CdS co-sensitized solar cell based on double-layered TiO_2 flower-rod substrate provides a novel strategy to construct QDSSCs.

2. Experimental

2.1. Materials

Titanium butoxide ($Ti(OC_4H_9)_4$), concentrated hydrochloric acid (HCl, 36.5–38 wt%), sodium chloride (NaCl), cadmium nitrate ($Cd(NO_3)_2{\cdot}4H_2O$), sodium sulfide ($Na_2S{\cdot}9H_2O$), selenium powder (Se), sodium sulfite (Na_2SO_3), sulfur powder (S), potassium chloride (KCl) and chloroplatinic acid ($H_2PtCl_6{\cdot}6H_2O$) were purchased from Tianjin Chemical Reagents Co. Ltd. All the chemicals are of analytic grade and used directly in experiments without further purification. Deionized water (DI water, resistivity of 18.2 MΩ cm) was obtained from MilliQ ultra-pure water system (Millipore, USA).

2.2. Preparation of hierarchical double-layered TiO_2 flower-rod substrates

Hierarchical double-layered TiO_2 flower-rod film on FTO glass was prepared by a facile hydrothermal process which is summarized in Supplementary information (Fig. S1a–c), details of the fabrication steps is similar to that described by Liu and Aydil [34]. Typically, Fluorine-doped tin dioxide (FTO) conducting glasses were thoroughly cleaned by sonication in a mixed solution of DI water, acetone, and isopropanol (volume ratios of 1: 1: 1) for 30 min, and finally dried in air. Then the well-cleaned FTO conducting glass was transferred to the Teflon-lined stainless steel autoclave at an angle against the wall of the Teflon-liner with the conductive side facing up (Fig. S1a). Subsequently, a transparent mixed solution consisted of 25 ml of DI water, 30 ml of concentrated hydrochloric acid, 5 ml of saturated NaCl aqueous solution and 1 ml of titanium butoxide was added into the Teflon-lined stainless steel autoclave, filling the 80% volume of the autoclave. Following this step, the hydrothermal synthesis reaction was conducted at the temperature of 150 °C for 12 h in an electric oven to form double-layered TiO_2 flower-rod film (Fig. S1b). After the completion of the hydrothermal reaction, the autoclave was cooled to room temperature under flowing water and the product was taken out, rinsed thoroughly with DI water and ethanol respectively. Finally, the product was dried in ambient air waiting to be sensitized with QDs (Fig. S1c). As a control, the well-cleaned FTO glass was put into the autoclave with the conductive side facing down under the identical reaction condition to obtain TiO_2 nanorod arrays.

2.3. Hierarchical TiO_2 flower-rod sensitized with CdS and CdSe QDs

In situ chemical bath deposition (CBD) is used to assemble CdS and CdSe onto a TiO_2 flower-rod film to form CdSe/CdS/TiO_2 structure (see the Supplementary information, Fig. S1d). For sensitization of CdS QDs, the CBD method resembles the procedure described in a previous paper [35]. Typically, a TiO_2 flower-rod film was dipped into a 0.1 M $Cd(NO_3)_2$ ethanol solution for 5 min, to allow Cd^{2+} ions to adsorb over TiO_2 flower-rod structure, and rinsed with ethanol to remove the excess Cd^{2+} ions, then dipped for another 5 min into a 0.1 M Na_2S methanol solution to allow S^{2-} to react with the Cd^{2+}, leading to the formation of CdS, and rinsed again with methanol. The two-step dipping procedure is termed as one CBD cycle, and the incorporated amount of CdS can be increased by repeating the assembly cycles. For CdSe QDs, sodium selenosulphate (Na_2SeSO_3) aqueous solution which was prepared by refluxing 0.3 M Se in 0.6 M Na_2SO_3 at 90 °C for about 6 h is used as the Se source for CBD. The CBD process of CdSe is similar to that of CdS but a longer time (15 min) is required for dipping the sample in the Na_2SeSO_3 solution. The sensitization process is shown as follows:

$$TiO_2 \xrightarrow{Cd^{2+}} Cd^{2+}/TiO_2 \rightarrow Wash \xrightarrow{S^{2-}} CdS/TiO_2 \rightarrow Wash \quad (1)$$

$$CdS/TiO_2 \xrightarrow{Cd^{2+}} Cd^{2+}/CdS/TiO_2 \rightarrow Wash \xrightarrow{SeSO_3^{2-}} CdSe/CdS/TiO_2 \rightarrow Wash \quad (2)$$

The CdSe/CdS co-sensitized TiO_2 flower-rod electrodes were prepared with several CBD cycles to investigate the optimal combination of CdSe and CdS.

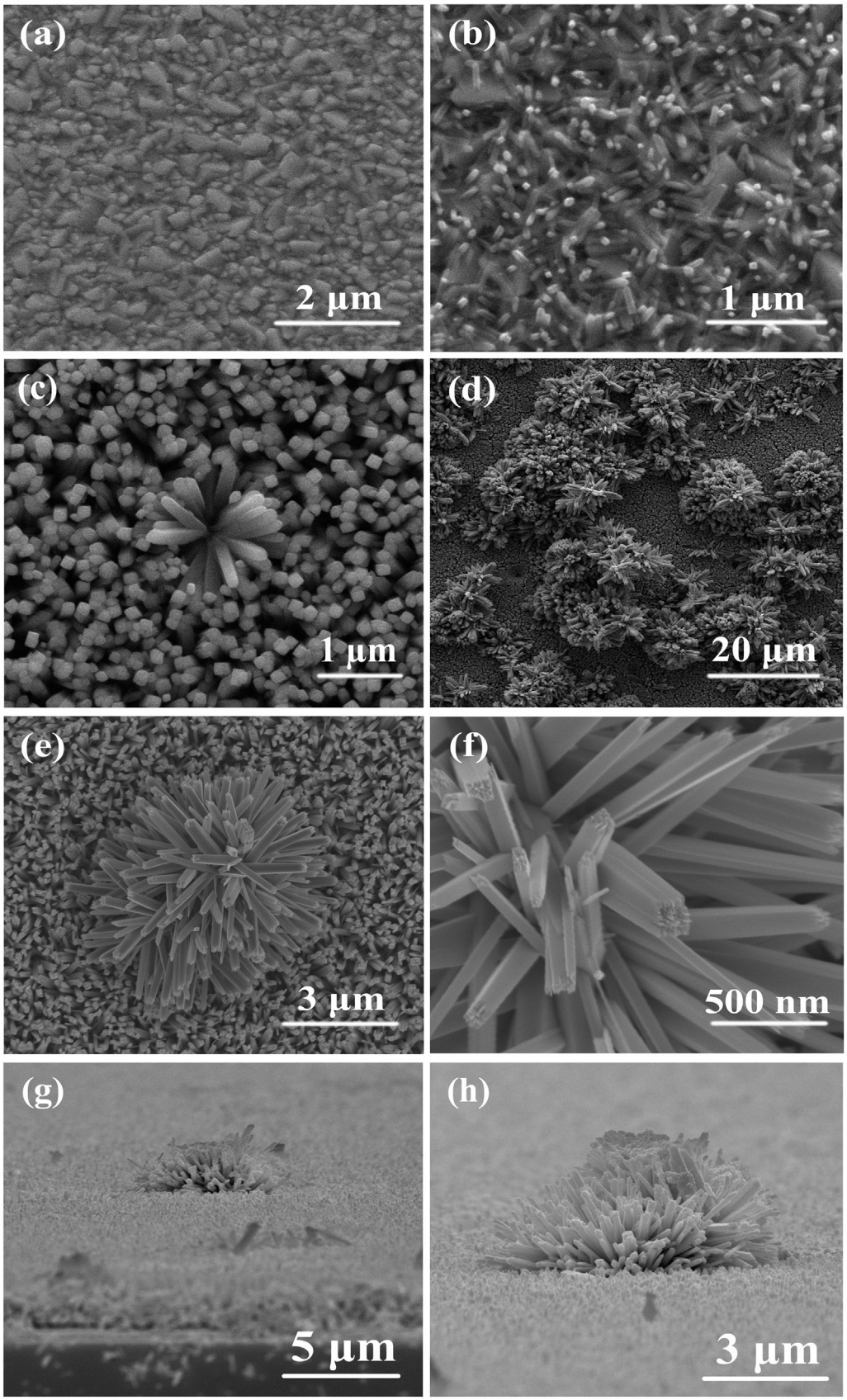

Fig. 1. FE-SEM images of TiO_2 flower-rod grown on FTO glass at 150 °C for (a) 0 h; (b) 4 h; (c) 8 h; and (d) 12 h. (e) Top view of the magnified TiO_2 flower-rod and (f) magnified view of flower; (g) cross-sectional view of TiO_2 flower-rod and (h) magnified view of (g).

2.4. Solar cell fabrication and photovoltaic measurements

The QDSSCs were assembled in a sandwich-type fashion with the Surlyn film of 60 μm thickness as spacer between QD-sensitized TiO_2 flower-rod photoanodes and Pt coated FTO counter electrodes, as depicted in the Supplementary information (Fig. S1e). Platinized counter electrodes were prepared by thermal decomposition of H_2PtCl_6 solution (5 mM in isopropanol) dropped onto FTO glass at 400 °C for 15 min. The polysulfide redox electrolyte, containing 0.6 M Na_2S, 0.2 M S and 0.2 M KCl [36] in the co-solvent of water and methanol with volume ratio of 7:3, in which the S^{2-} works as holes scavenger [37], was injected into the solar cell through the predrilled hole on the counter electrode. Finally, the drilled hole was sealed. The purpose of using co-solvent is to decrease the surface tension of the electrolyte solution, which is favorable for the penetration of the electrolyte into the TiO_2 film [38].

The photocurrent density–voltage (J–V) properties of the QDSSCs were obtained under illumination with sunlight simulator at AM 1.5 G (100 mW cm^{-2}) condition. The illuminated area of all the QDSSCs was fixed to 0.16 cm^2 by covering a mask. The incident photon to current conversion efficiency (IPCE) as a function of wavelength was monitored by employing a monochromator to select the illumination wavelength, a 500 W xenon arc lamp (Oriel) served as a light source.

2.5. Characterization

The crystal phases of the samples were characterized by X-ray diffraction (XRD), in a 2θ range from 10° to 90°, using CuKα radiation ($\lambda = 1.5416$ Å). The morphologies and lattice structures of the samples were examined with field-emission scanning electron microscope (FE-SEM, Nanosem 430 FEI, USA), transmission electron microscopy (TEM, Tecnai G2 F20 FEI, USA), high-resolution TEM (HR-TEM) and selected area electron diffraction (SAED). To prepare TEM sample, the QDs sensitized TiO_2 flower-rod film scraped from the FTO glass was dispersed in ethanol and sonicated, then a few drops of the solution were dropped onto a carbon film supported copper grid. The elemental compositions of the samples were analyzed by energy dispersive spectroscopy (EDS). The optical absorption spectra of bare TiO_2 flower-rod and QD-sensitized TiO_2 flower-rod electrodes were recorded in the range from 250 to 800 nm by UV–vis spectrometer. Nitrogen adsorption–desorption isotherm and BET surface area analysis were obtained using Micromeritics ASAP 2020.

3. Results and discussion

3.1. The formation of hierarchical TiO_2 flower-rod structure

The hierarchical double-layered TiO_2 flower-rod film directly grown on FTO glass has been synthesized using a facile hydrothermal method with the conductive side facing up. Morphologies of this TiO_2 flower-rod have been recorded by field-emission scanning electron microscope (FE-SEM). Fig. 1a and b are FE-SEM images of the FTO glass and the TiO_2 architecture grown at 150 °C for 4 h, respectively. It can be clearly seen that the surface of the FTO glass is covered sparsely with TiO_2 nanorods after 4 h of hydrothermal reaction (Fig. 1b), indicating that TiO_2 nanorods are firstly formed at the initial stage of hydrothermal reaction. The diameter of the formed TiO_2 nanorods is small, and the nanorod arrays have not fully covered the entire surface of FTO glass due to the insufficient reaction time. As presented in Fig. 1b, some bare FTO glass still can be observed after 4 h of hydrothermal reaction. Fig. 1c shows the top view of TiO_2 architecture grown for 8 h, it can be seen that parts of the flower are formed on the top of the nanorods, providing the proof of the formation of hierarchical TiO_2 flower-rod structure. With the proceeding of the hydrothermal reaction, more TiO_2 flowers can be formed on the top of TiO_2 nanorods as shown in Fig. 1d.

Fig. 1e shows the typical morphology of double-layered TiO_2 flower-rod structure. It reveals that the hierarchical architecture is constructed with two parts: one is 3D flower on the top and the other is 1D nanorod arrays at the bottom. In addition, it can also be seen that the 3D flower is composed of radially packed 1D nanorods, which numerous nanorods extended outside, and became gradually compact inside, meaning that the flowers may be formed from the aggregation of TiO_2 nanorods. Obviously, this open structure can enlarge the surface area of the TiO_2 film and enhance the QDs loading. Fig. 1f is the magnified view of TiO_2 flower, showing that the nanorods that constitute the 3D flower are in tetragonal shape with square top facets, which reveals the typical growth habit of the tetragonal crystal structure. The cross-sectional image of double-layered TiO_2 flower-rod is shown in Fig. 1g, it can be clearly seen that the 3D TiO_2 flower is on the top of 1D TiO_2 nanorod arrays. The well-aligned 1D nanorods as the bottom layer are nearly vertically grown on the FTO glass (see the Supplementary information, Fig. S2). Fig. 1h is the magnified view of Fig. 1g, which provides another evidence for the formation of TiO_2 flower on the top of nanorods layer. In addition, only single-layered TiO_2 nanorod arrays on FTO glass has also been fabricated under the identical hydrothermal reaction condition with the conductive side of FTO glass facing down. These TiO_2 nanorods are highly ordered and nearly perpendicular to the FTO substrate (see the Supplementary information, Fig. S3).

Although the reason leads to the formation of hierarchical TiO_2 flower-rod is not very clear to us, a possible formation mechanism of the TiO_2 flower-rod based on random aggregation of regrowth nanorods is proposed, which is illustrated in Fig. 2. The formation of the hierarchical TiO_2 architecture may experience several stages during the hydrothermal reaction including growth of nanorods underlayer, part dissolution of nanorods, and aggregation of the random regrowth nanorods on the top of nanorods layer. Initially, titania nucleus were formed on the surface of the FTO glass due to the slow hydrolysis of $Ti(OC_4H_9)_4$ in the acidic solution. At the same time, the adsorption of Cl^- provided by saturated NaCl on the nucleus favors its anisotropic growth to form 1D nanorods. The chemical reaction can be described as follows [11,12].

$$Ti^{4+} + nH_2O \rightarrow Ti(OH)_n^{4-n} + nH^+ \quad (3)$$

$$Ti(OH)_n^{4-n} \rightarrow Ti(IV)\ \text{oxo species} \rightarrow TiO_2 \quad (4)$$

The Ti(IV) oxo species is assumed to be an intermediate between TiO^{2+} and TiO_2, consisting of partly dehydrated polymeric Ti(IV) hydroxide [39]. The acid condition could slow down the hydrolysis reaction of $Ti(OC_4H_9)_4$ by providing free H^+ as present in reaction (3), which is necessary for the growth of oriented 1D TiO_2 nanorods. Meanwhile, Cl^- could preferentially adsorb on rutile (110) plane and retard the growth rate of (110) surface, which will facilitate the anisotropic growth of rutile nanorods along [001] orientation [40,41]. The growth of nanorods are well oriented and nearly perpendicular to the substrate. With the extension of the hydrothermal reaction time, the crystal growth rate starts to decrease, and part of the crystals may begin to dissolve to form the Ti(IV) oxo species again. At the same time, the Ti(IV) oxo species would diffuse to the solution and provide conditions for the random regrowth of nanorods. Subsequently, with the reaction proceeds, the supersaturation of Ti(IV) oxo species gradually reduced. From the kinetics viewpoint of crystal growth, low degree of supersaturation

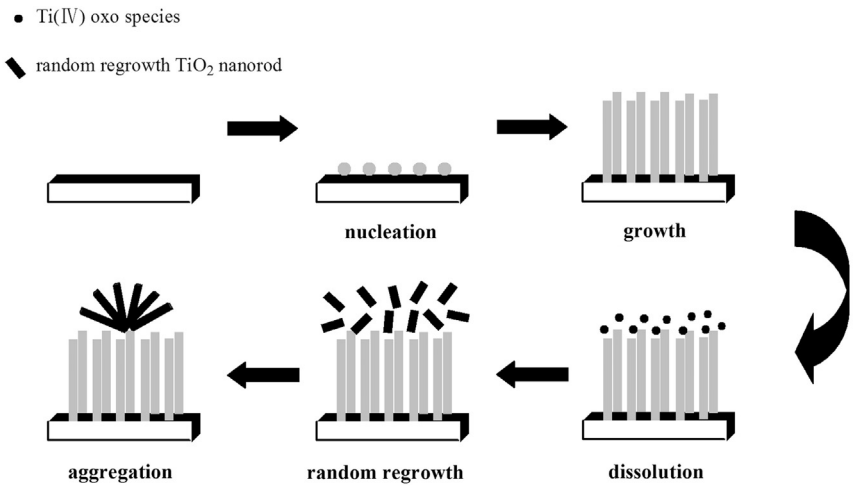

Fig. 2. The formation process of the hierarchical TiO_2 flower-rod structure.

promoted the formation of rutile nanorod aggregated objects [12], hence the random regrowth of the nanorods are inclined to aggregate to form the core of the flowers. As the hydrothermal reaction further prolonging, these aggregated nanorods would develop bigger, leading to the formation of flowers and randomly aggregated on the top of formed nanorods layer. Finally, the double-layered TiO_2 flower-rod structure is obtained by this hydrothermal method.

The crystal phases of the FTO glass and TiO_2 flower-rod electrodes have been characterized by X-ray diffraction (XRD), which is shown in the Supplementary information (Fig. S4). It is worth noting that all the characteristic peaks of TiO_2 flower-rod in the XRD patterns can be indexed to the tetragonal rutile phase of TiO_2 (JCPDS no. 21-1276), and the FTO glass also shows rutile structure (JCPDS no. 41-1445). The small lattice mismatch between FTO glass and rutile TiO_2 makes it possible to grow TiO_2 flower-rod on FTO glass. The sharpness of the diffraction peaks implies a high crystallinity of the TiO_2 flower-rod film. Compared with the other diffraction peaks in XRD patterns of the as-prepared TiO_2 flower-rod, the enhanced (002) peak indicates that the hierarchical TiO_2 architecture is highly oriented with respect to the substrate surface and grow along the [001] direction with the growth axis parallel to the substrate surface.

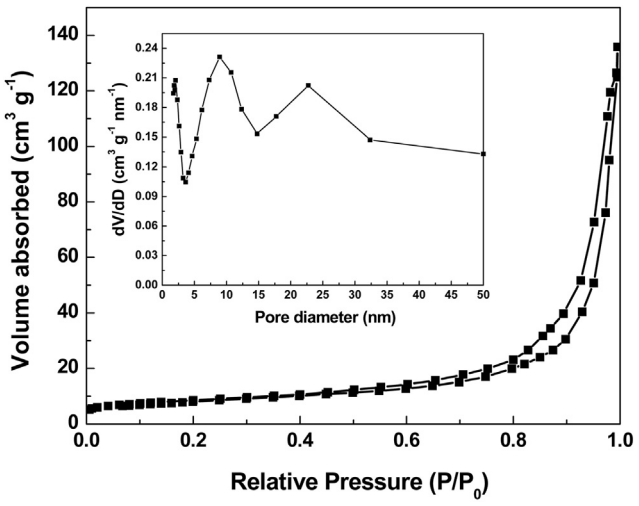

Fig. 3. N_2 adsorption–desorption isotherm of the as-prepared TiO_2 flower-rod. The inset shows the pore size distributions calculated using the BJH method.

The mesoporous nature of the TiO_2 flower-rod has been quantified with N_2 adsorption–desorption measurements and the corresponding pore size distribution is shown in Fig. 3. The estimated pore volume of the TiO_2 flower-rod is 0.1951 $cm^3\ g^{-1}$. The pore size distribution, as shown in the inset of Fig. 3, shows a range between 5 and 35 nm, and the average pore diameter is calculated by BJH method to be 26.3 nm. The BET surface area of 28.8891 $m^2\ g^{-1}$ is obtained with the TiO_2 flower-rod, which is higher than that of TiO_2 nanorod (19.7655 $m^2\ g^{-1}$). The increased BET surface area of the TiO_2 flower-rod indicates that more QDs can be adsorbed on to the surface of the TiO_2 flower-rod, which may be favorable for improving the performance of QDSSCs.

3.2. Characterization of CdSe/CdS/TiO_2 flower-rod structure

Fig. 4 shows FE-SEM images of bare TiO_2 flower-rod and CdSe/CdS/TiO_2 flower-rod structures as well as their respective elemental composition. As shown in Fig. 4a, the bare TiO_2 flower-rod exhibits a smooth surface. The elemental composition analysis of TiO_2 flower-rod from EDS in Fig. 4b shows that Ti and O are dominant elements, confirming that the composition of this hierarchical structure was mainly composed of TiO_2. Other elements including Si and Sn come from FTO glass can also be identified by EDS, but in a relatively low level. After sensitization with CdS and CdSe nanocrystals, the surface of TiO_2 flower-rod became rougher than that of bare TiO_2 flower-rod as shown in Fig. 4c, which means that the QDs have been successfully deposited on the surface of the TiO_2 flower-rod after CBD. Fig. 4d is the higher magnification image of QD-sensitized TiO_2 flower-rod. It can be seen that small nanoparticles are distributed on the top of TiO_2 flower and the surface of each nanorod that constituted the TiO_2 flower. In Fig. 4e, the appearance of characteristic peaks of S, Se, and Cd in the EDS of QD-sensitized TiO_2 flower-rod confirms that CdS and CdSe QDs are successfully assembled on the TiO_2 flower-rod.

The detailed microscopic characterization of the CdSe/CdS/TiO_2 flower-rod has been performed by transmission electron microscope (TEM), high-resolution TEM (HR-TEM), and selected area electron diffraction (SAED). Fig. 5a is the typical TEM image of the CdSe/CdS/TiO_2 flower-rod unit, it can be seen clearly that the surface of the flower-rod unit is covered by CdSe/CdS, which could further confirm that CdSe/CdS have been successfully deposited on TiO_2. From the apparent spot diffraction patterns shown in Fig. 5b,

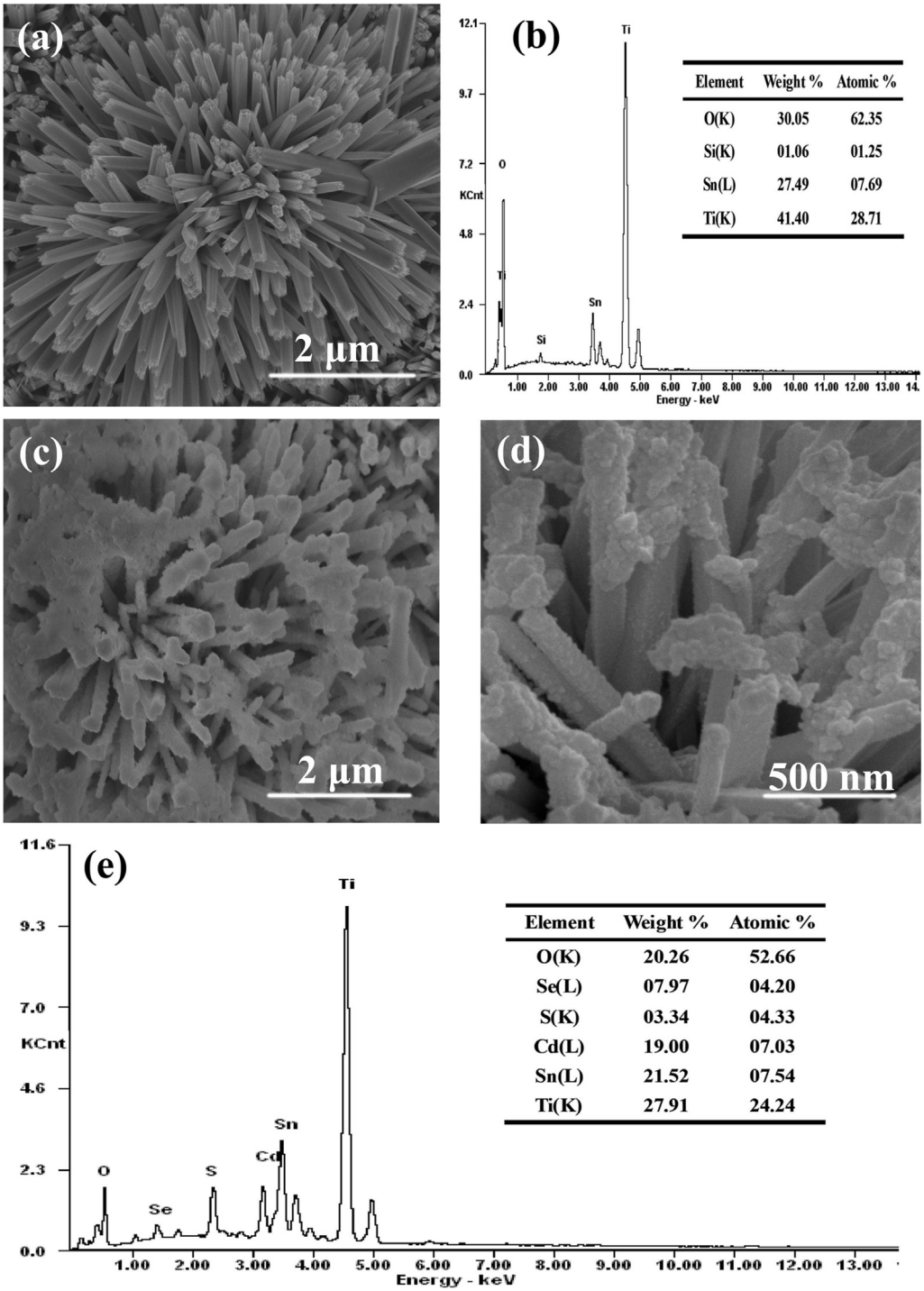

Fig. 4. (a) Morphology of bare TiO_2 flower-rod; (b) EDS spectra of the corresponding structure. (c) Morphology of CdSe/CdS/TiO_2 flower-rod at low magnification and (d) at high magnification; (e) EDS spectra of CdSe/CdS/TiO_2 flower-rod.

it can be observed that the well-aligned spots come from single-crystalline TiO_2 nanorod, and the diffraction rings originates from the polycrystalline of CdS and CdSe. Fig. 5c shows an HR-TEM image of the CdSe/CdS/TiO_2 flower-rod unit. The clear lattice fringes indicated high crystallinity of TiO_2, CdS and CdSe. The lattice spacing measured for the crystalline plane is 0.322 nm, corresponding to the (110) plane of rutile TiO_2 (JCPDS no. 21-1276). Among the crystal planes of rutile TiO_2, the (110) plane possesses the lowest surface energy [42]. According to the crystal growth theory, the planes with lower surface energies generally grow slowly and tend to survive during the growth [43]. Therefore, the (110) plane of the rutile TiO_2 can be obviously observed in the HR-TEM photographs. By carefully measuring the lattice parameters and comparing with the data in JCPD, the crystallites with lattice fringe of 0.336 nm connecting to TiO_2 can be ascribed to the (111) plane of CdS (JCPDS no. 10-0454), and outer crystallites close to the CdS layer with lattice spacing of 0.328 nm corresponds to the (101) plane of CdSe (JCPDS no. 08-0459). These results provide powerful

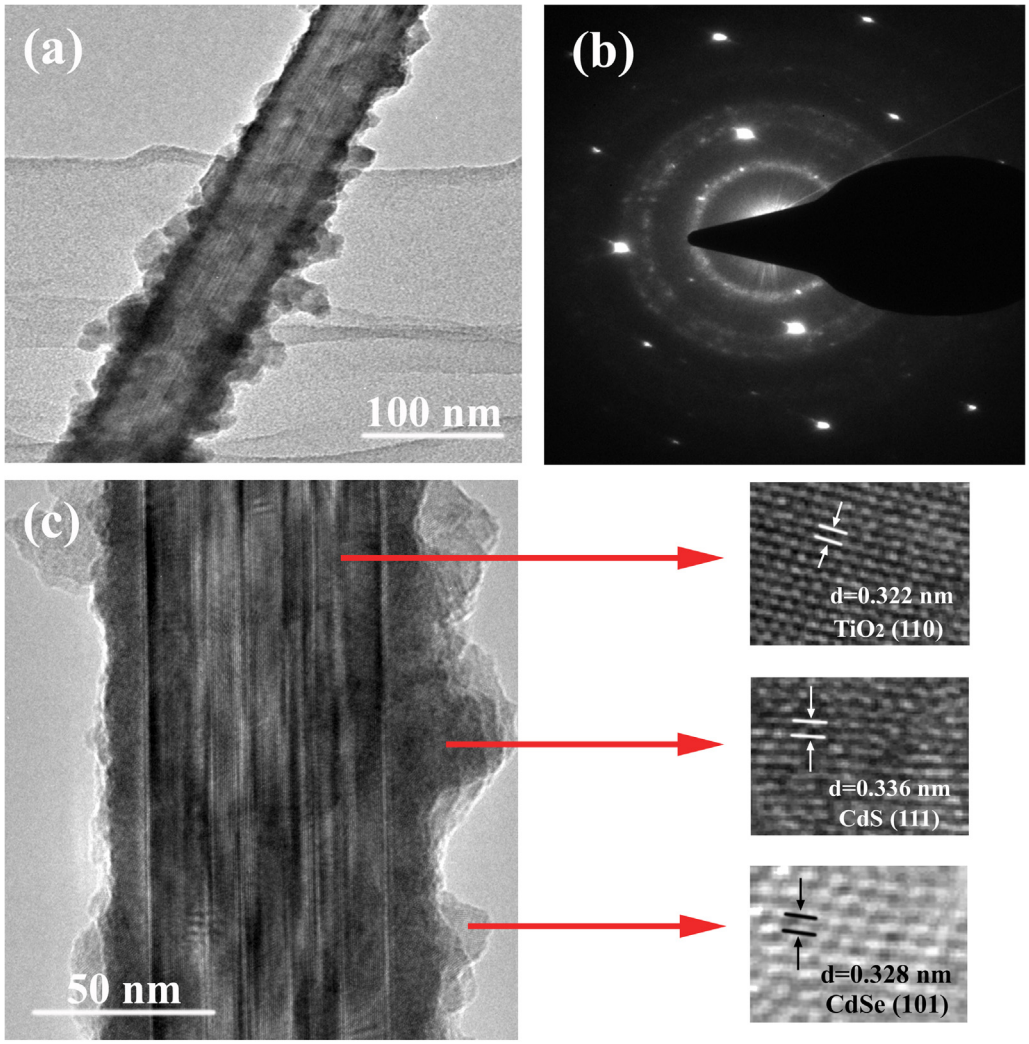

Fig. 5. (a) TEM image of CdSe/CdS/TiO_2 flower-rod unit; (b) SAED pattern of CdSe/CdS/TiO_2 flower-rod; (c) HR-TEM image of CdSe/CdS/TiO_2 flower-rod unit.

evidence for successful coating of CdS and CdSe QDs on the surface of TiO_2 flower-rod and the formation of CdSe/CdS/TiO_2 cascade structure.

3.3. Optical properties of QD-sensitized TiO_2 flower-rod electrodes

Light absorption properties of the bare TiO_2 flower-rod and QD-sensitized TiO_2 flower-rod electrodes are evaluated using the UV–vis spectrometer. As shown in Fig. 6, the absorption edge of bare TiO_2 flower-rod electrode (spectrum a, Fig. 6) occurs at around 410 nm and the main light absorption centered on ultraviolet light region, this can be ascribed to the wide band gap of rutile TiO_2 (3.0 eV) [44]. Compared with the absorption spectra of the bare TiO_2 flower-rod film, the absorption edges of the CdS/TiO_2 flower-rod and CdSe/TiO_2 flower-rod electrodes were enlarged to 530 nm (spectrum b, Fig. 6) and 650 nm (spectrum c, Fig. 6), corresponding to the calculated band gaps of 2.34 eV and 1.91 eV for CdS and CdSe, respectively. The calculated band gaps are higher than the values of bulk CdS (2.25 eV) and CdSe (1.70 eV), indicating that the sizes of CdS and CdSe deposited on the TiO_2 flower-rod film are within the scale of QDs. According to the empirical equations given by Yu et al. [45], the mean diameters of CdS and CdSe QDs were estimated to be 9.376 and 7.761 nm, respectively. In addition, the absorption intensity in visible light region increased after the deposition of CdS or CdSe on the TiO_2 flower-rod film.

For the CdSe/CdS co-sensitized TiO_2 flower-rod electrode (spectrum d, Fig. 6), a slight red-shift of the absorption edge can be observed compared with the absorption spectrum of CdSe/TiO_2 flower-rod electrode, and the absorbance is higher than that of CdS/

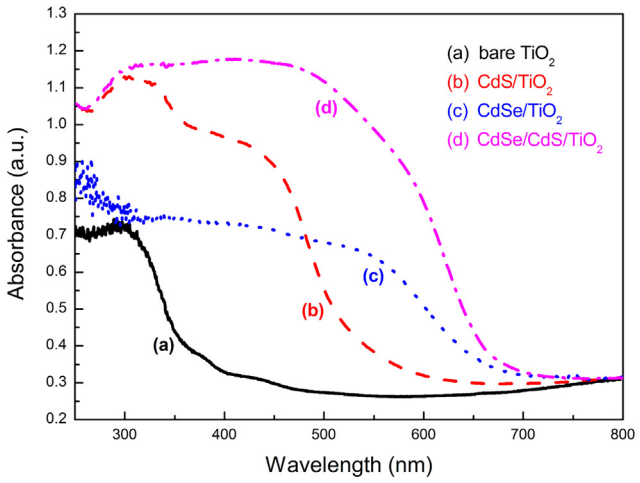

Fig. 6. Diffuse reflectance absorption spectra of bare TiO_2 flower-rod film and the TiO_2 flower-rod films sensitized with CdS, CdSe and CdSe/CdS QDs.

TiO_2 flower-rod and CdSe/TiO_2 flower-rod electrodes. In the short wavelength region (λ < 500 nm) where both CdS and CdSe are photoactive, the increase of absorbance can be attributed to co-absorption of both CdS and CdSe to the light. In the long wavelength region (500–700 nm), the higher absorbance of CdSe/CdS/TiO_2 flower-rod implies that more CdSe QDs were deposited on the co-sensitized electrode. This result also indicates that the deposition rate of CdSe on a CdS sensitized TiO_2 film is faster than on a bare TiO_2 film [46]. Therefore, the co-sensitization effect of CdS and CdSe can be observed by extension of the absorption range and the increase of absorbance.

3.4. Photoelectrochemical characterization

The incident photon to current conversion efficiency (IPCE) spectra of single CdS, CdSe sensitized, and CdSe/CdS co-sensitized solar cells are presented in Fig. 7. The light response revealed by the IPCE spectra of CdS/TiO_2 flower-rod, CdSe/TiO_2 flower-rod, and CdSe/CdS/TiO_2 flower-rod solar cells exhibit similar trends to their corresponding UV–vis spectra in Fig. 6. The maximum IPCE values obtained from CdS/TiO_2 flower-rod and CdSe/TiO_2 flower-rod solar cells are around 35% and 20%, respectively. Furthermore, the maximum IPCE value is improved to 48% with the CdSe/CdS/TiO_2 flower-rod solar cell, which is ascribed to the joint contribution from CdS and CdSe QDs in the light harvest. According to Ref. [47], IPCE is determined by three factors:

$$\mathrm{IPCE} = \mathrm{LHE} \cdot \eta_{\mathrm{inj}} \cdot \eta_{\mathrm{cc}} \tag{5}$$

where LHE is the light harvesting efficiency, η_{inj} is the charge injection efficiency, and η_{cc} is the charge collection efficiency. For the CdSe/CdS/TiO_2 flower-rod solar cell, the light response region is enlarged compared with that of single CdS or CdSe sensitized solar cell based on TiO_2 flower-rod, resulting in the enhancement of the light harvesting efficiency (LHE). In addition, the introduction of a CdS layer between TiO_2 and CdSe can elevate the conduction band edge of CdSe, giving a higher driving force for the injection of excited electrons of CdSe layer [46], causing an increment of the charge injection efficiency (η_{inj}). Moreover, the insertion of CdS layer can also trigger the redistribution of the electrons between CdS and CdSe to form a stepwise conduction band edges in the order of TiO_2 < CdS < CdSe, which is helpful to the collection of photoexcited electrons from CdSe to inject into TiO_2 [48], leading to an increased collection efficiency (η_{cc}). Therefore, a significantly enhanced IPCE is obtained with CdSe/CdS/TiO_2 flower-rod solar cell compared with that of CdS/TiO_2 flower-rod and CdSe/TiO_2 flower-rod solar cells.

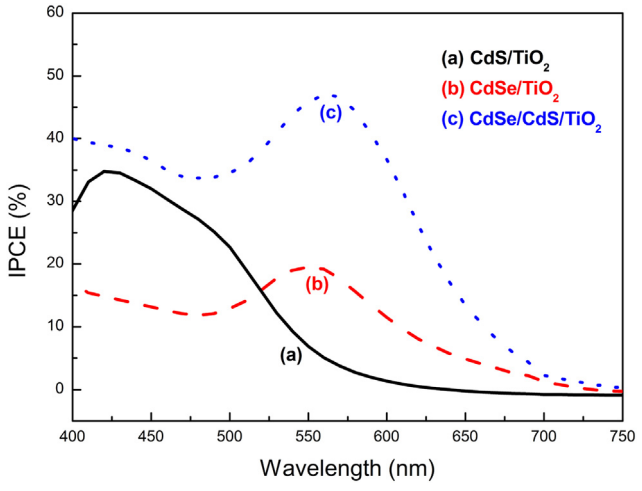

Fig. 7. IPCE spectra of single CdS, CdSe sensitized, and CdSe/CdS co-sensitized TiO_2 flower-rod solar cells.

The photocurrent density–voltage (J–V) curves of QDSSCs assembled with different photoanodes were measured by Oriel I–V test station under one sun condition (AM 1.5 G, 100 mW cm^{-2}) with the active area of 0.16 cm^2. Fig. 8a displays the J–V characteristics of TiO_2 flower-rod solar cells sensitized by different CBD cycles of CdS QDs. It is found that both the short-circuit current density (J_{sc}) and open-circuit voltage (V_{oc}) increased gradually with the increase of the CdS QDs cycles at initial stage (from 5 cycles to 9 cycles), then further increase of CBD cycles of CdS QDs (from 9 cycles to 11 cycles) leads to the reduction of the J_{sc} and V_{oc}. The variation trend of J_{sc} and V_{oc} as a function of CdS QDs cycles are shown in Fig. 8b and c, it can be observed that 9 cycles of CdS QDs on TiO_2 flower-rod make the solar cell exhibit the best photovoltaic performance. Based on this optimal cycles of CdS QDs, different CBD cycles of CdSe QDs decorated CdS(9)/TiO_2 flower-rod are investigated to seek the influence of CdSe layers on the performance of the co-sensitized solar cells. Fig. 8d shows the variation of J–V curves with the increase of CdSe QDs cycles on CdS(9)/TiO_2 flower-rod solar cells. Significant improvement of J_{sc} is observed as the CdSe cycles increase from 2 to 6. Appropriate increase of CBD cycles can enlarge the loading amount of CdSe QDs, which results in more light absorption to generate photoexcited electrons. A slight enhancement of V_{oc} also occurs with the increase of CdSe QDs cycles, which can be explained according to the following equation discussed in Refs. [49,50].

$$V_{\mathrm{oc}} = \frac{E_{\mathrm{Fn}} - E_{\mathrm{redox}}}{e} = \frac{k_B T}{e} \ln(n/n_0) \tag{6}$$

where E_{Fn} is the quasi-Fermi level of the electrons in semiconductor photoanode under illumination; E_{redox} is the potential of redox electrolyte; e is the positive elementary charge; k_BT is the thermal energy; n is the electron concentration in conduction band of the semiconductor photoanode under illumination; n_0 is the electron concentration in the dark condition. When the CdSe QDs cycles increase from 2 to 6 cycles, more electrons would be injected into the conduction band of TiO_2 under illumination and the value of n is increased, leading to more negative shift of the E_{Fn}, while the E_{redox} remains unchangeable, causing the improvement of V_{oc}. However, both J_{sc} and V_{oc} are found to decrease when the CBD cycles of CdSe QDs are further increased. This phenomenon can be explained in three ways: Firstly, the excessive CBD deposition cycles would cause the aggregation of CdSe QDs and form excessive grain boundaries between CdSe nanoparticles. These grain boundaries can act as potential barrier for charge transfer to enhance the possibilities of the recombination between electrons and holes, leading to a decrease in the overall efficiency. Secondly, the excessive CBD cycles can lead to the growth of CdSe QDs, resulting in the poor charge injection efficiency caused by the reduced size quantization of the large QDs [51], moreover, the oversized CdSe particles will lose the dominance as QDs (large extinction coefficients and generating multiple electron–hole pairs). Finally, the excessive CBD cycles may hinder the diffusion of the electrolyte due to the local block caused by aggregation of CdSe QDs, which limit the efficiency of charge separation and charge extraction. The evolution of power conversion efficiency (η) with CBD cycles of CdSe QDs is shown in Fig. 8e. It is found that the value of η increased first (from 2 to 6 cycles), and then decreased (from 6 to 8 cycles), and the maximum value of η is obtained with CdSe(6)/CdS(9)/TiO_2 flower-rod combination.

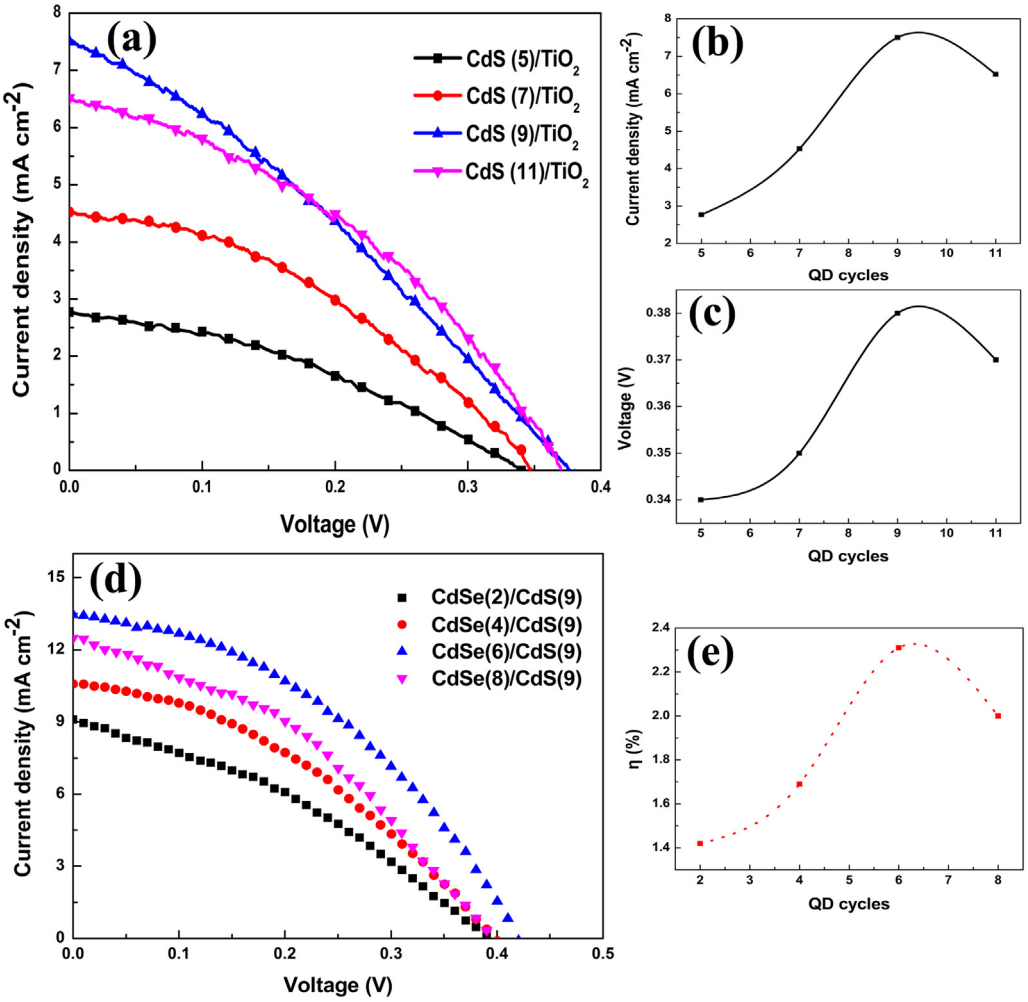

Fig. 8. (a) Photocurrent density–voltage (J–V) characteristics of different CBD cycles of CdS QDs sensitized TiO_2 flower-rod solar cells; (b) and (c) variation of the current density and voltage as a function of CBD cycles of CdS QDs, respectively. (d) J–V curves of different CBD cycles of CdSe QDs on CdS(9)/TiO_2 flower-rod solar cells; and (e) variation of the power conversion efficiency as a function of CBD cycles of CdSe QDs.

In order to demonstrate that the unique TiO_2 flower-rod structure has important effect for improvement of J–V performance in CdSe/CdS QDSSCs, we also compare the J–V behaviors of the CdSe/CdS QDSSCs based on TiO_2 nanorod and TiO_2 flower-rod structure sensitized with the same cycles of CdSe/CdS, which is shown in the Supplementary information (Fig. S5). In contrast with CdSe/CdS/TiO_2 nanorod solar cell, both the J_{sc} and V_{oc} of CdSe/CdS/TiO_2 flower-rod solar cell are increased (from 10.72 mA cm^{-2} to 13.46 mA cm^{-2}; from 0.38 V to 0.42 V, respectively), resulting in the enhancement of power conversion efficiency from 1.63% to 2.31%, showing that the TiO_2 flower-rod structure is advantageous over the TiO_2 nanorod structure. The augment of J–V performance of the CdSe/CdS/TiO_2 flower-rod solar cell can be ascribed to the enlarged surface for more adsorption of QDs provided by the formation of flower-rod structure.

Fig. 9 compares the J–V curves of the single CdS, CdSe sensitized, and CdSe/CdS co-sensitized TiO_2 flower-rod solar cells at their optimal CBD cycles that illuminated in front-side, and the J–V curve of CdSe(6)/CdS(9)/TiO_2 flower-rod solar cell illuminated in back-side is also included. The corresponding photovoltaic performance parameters of these solar cells including short-circuit current density (J_{sc}), open-circuit voltage (V_{oc}), fill factor (FF), and power conversion efficiency (η) are listed in Table 1. The photovoltaic performance of CdSe/CdS co-sensitized TiO_2 flower-rod

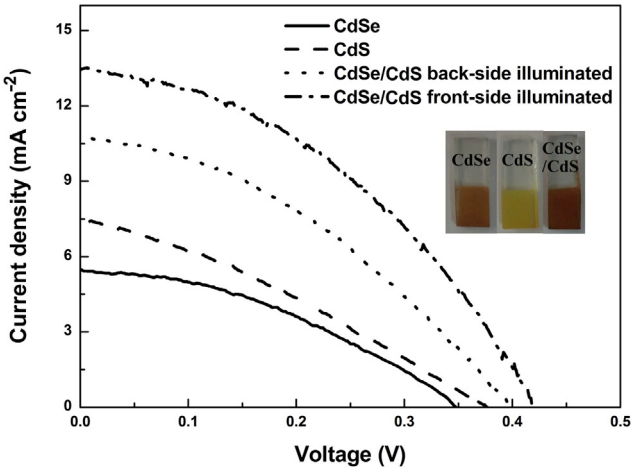

Fig. 9. Photocurrent density–voltage (J–V) curves of QDSSCs assembled with CdSe/TiO_2 flower-rod, CdS/TiO_2 flower-rod, CdSe/CdS/TiO_2 flower-rod (back-side illuminated), and CdSe/CdS/TiO_2 flower-rod (front-side illuminated) electrodes measured under AM 1.5 G condition. The insets are the digital photographs of the corresponding electrodes.

Table 1
Photovoltaic parameters of QDSSCs based on TiO_2 flower-rod solar cells.

Electrode (CdSe/CdS)	J_{sc} (mA cm^{-2})	V_{oc} (V)	FF	η (%)
6c/0c	5.48	0.35	0.38	0.73
0c/9c	7.50	0.38	0.38	1.08
6c/9c (back-side)	10.79	0.40	0.40	1.73
6c/9c (front-side)	13.46	0.42	0.41	2.31

solar cell is superior to single CdS or CdSe sensitized TiO_2 flower-rod solar cells, which can be ascribed to the complementary effect of these two kinds of QDs in the extension of light absorption range and charge injection from QDs to TiO_2. The power conversion efficiency of CdSe/CdS/TiO_2 flower-rod front-side illuminated solar cell can reach to 2.31%, which is 216.44% higher than that of CdSe/TiO_2 flower-rod solar cell, and 113.89% higher than that of CdS/TiO_2 flower-rod solar cell. Furthermore, the TiO_2 flower-rod photoanode and Pt counter electrode that assembled the QDSSCs are both prepared on FTO glass, which means that the assembled solar cell can be illuminated from the side of TiO_2 photoanode (front-side) or Pt counter electrode (back-side). We consider that front-side illumination can make full use of light due to more incident light can pass through the sensitized TiO_2 electrode to induce more photoelectrons from sensitizers, which is helpful to improve the performance of solar cells, while the back-side illumination solar cells may result in relatively low efficiency due to the bad use of light. With this consideration, the comparison of QDSSCs with front-side and back-side illumination is also provided in Fig. 9. The power conversion efficiency of 1.73% is obtained with CdSe(6)/CdS(9)/TiO_2 flower-rod solar cell under back-side illumination, which only approaches 75% that of front-side illumination (2.31%). This reduced power conversion efficiency mainly results from the undesirable light absorption of the electrolyte and unwanted reflection of light by the Pt counter electrode. The relative higher power conversion efficiency obtained with CdSe(6)/CdS(9)/TiO_2 flower-rod solar cell under front-side illumination indicates that a more efficient use of light will contribute to the improvement of photovoltaic performance of QDSSCs, and the potential value of this TiO_2 flower-rod film on transparent FTO glass as front-side illuminated photoanode in designing high efficiency of QDSSCs.

Several reasons may be responsible for the enhanced photovoltaic performance of CdSe/CdS/TiO_2 flower-rod front-side illuminated solar cell. First, hierarchical TiO_2 flower-rod architectures not only retain the advantages of efficient charge separation and transport properties provided by 1D nanorods, but also increase the deposition of QDs with the enlarged surface area provided by 3D TiO_2 flower on the top of 1D nanorod arrays, which increase the absorption of light. In addition, another function of 3D flower is that it can be used as a scattering layer to enhance the utilization of light. The effect of the hierarchical TiO_2 flower-rod on light absorption is depicted in Fig. 10a. It can be seen that this hierarchical architecture can lead to more deposition of QDs and reflect the incident light which pass through the gaps among nanorods, resulting in the improvement of the light harvesting efficiency. Second, a cascade structure is formed as the sequential deposition of CdS and CdSe onto the TiO_2 flower-rod film, which would result in the Fermi level alignment caused by the electrons flow from high energy level of CdS to low energy level of CdSe. This Fermi level alignment would force the band edge of CdS downward shift and the band edge of CdSe upward shift, forming a stepwise band edges in the order of TiO_2 < CdS < CdSe [46], which is shown in Fig. 10b. An efficient charge transfer channel would be provided by the stepwise band edge structure, which is advantageous to the electron injection and hole-recovery of CdS and CdSe. Moreover, CdSe outer layer of the stepwise structure can act as the energy barrier at the interface between the CdS and the electrolyte to prevent the electrons transport back to the electrolyte, and the heterojunction formed between TiO_2 and CdS is helpful to collect excited electrons from CdSe to inject into TiO_2, leading to the improvement of power conversion efficiency. Third, compared with single QD-sensitized TiO_2 flower-rod electrodes, the CdSe/CdS co-sensitized TiO_2 flower-rod electrode exhibits broader absorption range and higher absorbance, which greatly raised the utilization of the solar energy.

The stability of CdSe(6)/CdS(9)/TiO_2 flower-rod front-side illuminated solar cell has been monitored at different time intervals, and the results are shown in Fig. 11. About 15% degradation of η is observed after 120 h. Two possible reasons may be responsible for the decrease of η, one is the photoanodic corrosion [37], and the other is the poisoning effects [52] induced by the adsorption of sulfide ions in polysulfide electrolyte on the surface of Pt counter electrode. Several studies indicate that introduce a ZnS passivation layer onto the surface of the QDs sensitizer can protect QDs materials from photocorrosion and improve the cell efficiency and stability [53]. In addition, it is reported that copper sulfide (Cu_2S and CuS) counter electrode exhibits high stability, low resistance, and high catalytic activity in QDSSCs using polysulfide electrolyte as redox couple [54]. Therefore, further improvement of photovoltaic performance in QDSSCs is possible by developing appropriate

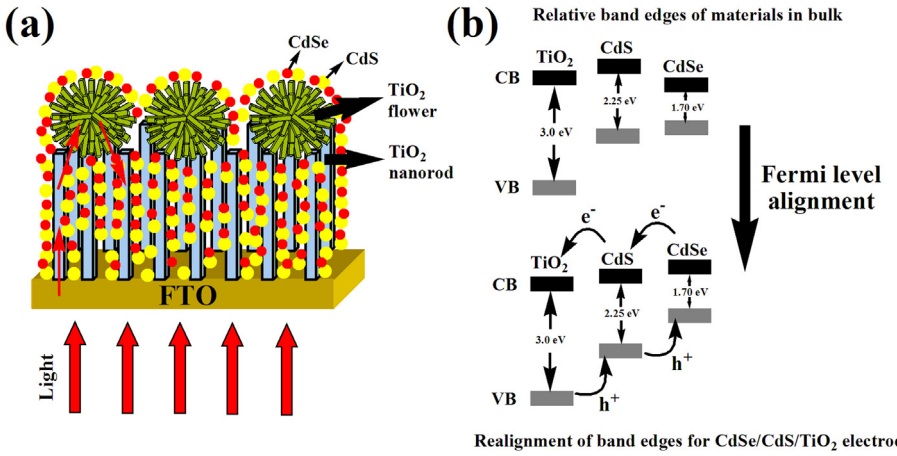

Fig. 10. (a) Schematic diagram of the light capture of TiO_2 flower-rod structure; (b) Stepwise band edge structure of CdSe/CdS/TiO_2 electrode after redistribution of electrons between CdS and CdSe (defined as Fermi level alignment for bulk materials) for efficient transport of the excited electrons and holes.

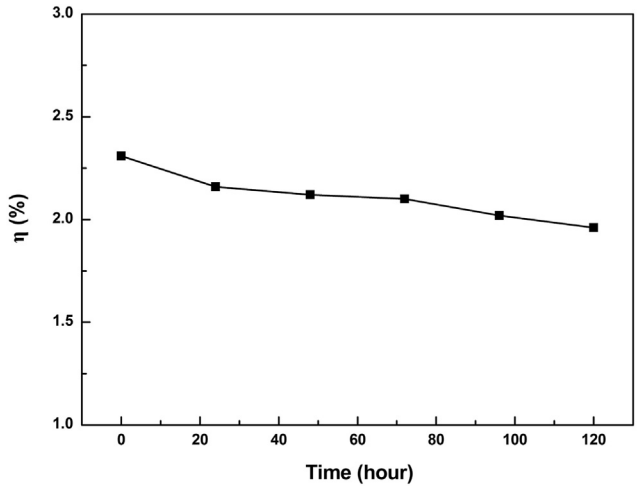

Fig. 11. Variation of the power conversion efficiency of CdSe(6)/CdS(9)/TiO_2 flower-rod front-side illuminated solar cell as a function of time.

passivation layer and new counter electrode materials with good electrocatalytic activity for the reduction of polysulfide electrolyte, which will be the focus of our continuous research work.

4. Conclusion

In summary, the hierarchical double-layered TiO_2 flower-rod film directly grown on FTO glass has been successfully synthesized by a facile hydrothermal method. The possible formation mechanism of this hierarchical architecture is also proposed based on random aggregation of regrowth nanorods. The hierarchical double-layered TiO_2 flower-rod film as substrate has been applied in CdSe/CdS co-sensitized solar cells. The effects of CdS and CdSe CBD cycles on the performance of QDSSCs have been systematically investigated and the optimal combination is found to be CdSe(6)/CdS(9). The CdSe/CdS/TiO_2 flower-rod solar cell shows broadened absorption range in visible light, increased absorbance and remarkable enhanced photovoltaic performance compared with single CdS or CdSe sensitized TiO_2 flower-rod solar cells. The power conversion efficiency of CdSe(6)/CdS(9)/TiO_2 flower-rod solar cell can reach to 2.31% under one sun illumination (AM 1.5 G, 100 mW cm^{-2}), which is significantly higher than that of CdSe/CdS/TiO_2 nanorod solar cell, showing that the unique double-layered TiO_2 flower-rod structure is advantageous over the single-layered TiO_2 nanorod structure in QDSSCs.

Acknowledgment

The authors gratefully acknowledge the support for this work from the Key Project of Tianjin Sci-Tech Support Program (no 08ZCKFSH01400).

Appendix A. Supplementary data

Supplementary data related to this article can be found at http://dx.doi.org/10.1016/j.jpowsour.2014.07.091.

References

[1] T. You, L. Jiang, K.L. Han, W.Q. Deng, Nanotechnology 24 (2013) 245401.
[2] J. Wang, T. Zhang, D. Wang, R. Pan, Q. Wang, H. Xia, J. Alloys Compd. 551 (2013) 82–87.
[3] Y. Ji, Mater. Lett. 108 (2013) 208–211.
[4] N. Huang, Y. Xie, B. Sebo, Y. Liu, X. Sun, T. Peng, W. Sun, C. Bu, S. Guo, X. Zhao, J. Power Sources 242 (2013) 848–854.
[5] C. Gu, C. Shannon, J. Mol. Catal. A Chem. 262 (2007) 185–189.
[6] G. Ji, Z. Liu, D. Guan, Y. Yang, Appl. Surf. Sci. 282 (2013) 695–699.
[7] D.H. Kim, W.M. Seong, I.J. Park, E.-S. Yoo, S.S. Shin, J.S. Kim, H.S. Jung, S. Lee, K.S. Hong, Nanoscale 5 (2013) 11725–11732.
[8] J. Xue, Q. Shen, W. Liang, X. Liu, F. Yang, Electrochim. Acta 97 (2013) 10–16.
[9] Z. Liu, H. Zhu, N. Song, T. Lian, Nano Lett. 13 (2013) 5563–5569.
[10] H. Zhu, J. Tao, T. Wang, J. Deng, Appl. Surf. Sci. 257 (2011) 10494–10498.
[11] J. Zhou, G. Zhao, G. Han, B. Song, Ceram. Int. 39 (2013) 8347–8354.
[12] J. Luo, L. Gao, J. Alloys Compd. 487 (2009) 763–767.
[13] L.-Y. Lin, M.-H. Yeh, C.-P. Lee, Y.-H. Chen, R. Vittal, K.-C. Ho, Electrochim. Acta 57 (2011) 270–276.
[14] Z. Li, L. Yu, Y. Liu, S. Sun, Electrochim. Acta 129 (2014) 379–388.
[15] L. Yu, Z. Li, Y. Liu, F. Cheng, S. Sun, Appl. Surf. Sci. 305 (2014) 359–365.
[16] Ö. Kerkez, İ. Boz, React. Kinet. Mech. Catal. 110 (2013) 543–557.
[17] P. Sudhagar, J.H. Jung, S. Park, Y.-G. Lee, R. Sathyamoorthy, Y.S. Kang, H. Ahn, Electrochem. Commun. 11 (2009) 2220–2224.
[18] R. Katoh, M. Murai, A. Furube, Chem. Phys. Lett. 461 (2008) 238–241.
[19] T. Lindgren, H. Wang, N. Beermann, L. Vayssieres, A. Hagfeldt, S.-E. Lindquist, Sol. Energy Mater. Sol. Cells 71 (2002) 231–243.
[20] K. Prabakar, H. Seo, M. Son, H. Kim, Mater. Chem. Phys. 117 (2009) 26–28.
[21] F. Qiao, Y. Sang, D. Kang, J. Mater. Sci. Mater. Electron. 24 (2013) 2636–2640.
[22] W. Yoon, J.E. Boercker, M.P. Lumb, D. Placencia, E.E. Foos, J.G. Tischler, Sci. Rep. 3 (2013) 2225.
[23] N. Guijarro, T. Lana-Villarreal, T. Lutz, S.A. Haque, R. Gómez, J. Phys. Chem. Lett. 3 (2012) 3367–3372.
[24] J. Tian, R. Gao, Q. Zhang, S. Zhang, Y. Li, J. Lan, X. Qu, G. Cao, J. Phys. Chem. C 116 (2012) 18655–18662.
[25] M.C. Beard, J. Phys. Chem. Lett. 2 (2011) 1282–1288.
[26] W.A. Tisdale, K.J. Williams, B.A. Timp, D.J. Norris, E.S. Aydil, X.-Y. Zhu, Science 328 (2010) 1543–1547.
[27] G. Zhu, L. Pan, T. Xu, Z. Sun, ACS Appl. Mater. Interfaces 3 (2011) 3146–3151.
[28] M. Grätzel, Nature 414 (2001) 338–344.
[29] M. Li, Y. Liu, H. Wang, H. Shen, W. Zhao, H. Huang, C. Liang, J. Appl. Phys. 108 (2010) 094304.
[30] S.S. Kalanur, Y.J. Hwang, O.-S. Joo, J. Colloid Interface Sci. 402 (2013) 94–99.
[31] H. Wang, C. Luan, X. Xu, S.V. Kershaw, A.L. Rogach, J. Phys. Chem. C 116 (2012) 484–489.
[32] F.B. Nisanci, Ü. Demir, Langmuir 28 (2012) 8571–8578.
[33] C. Gu, H. Xu, M. Park, C. Shannon, Langmuir 25 (2009) 410–414.
[34] B. Liu, E.S. Aydil, J. Am. Chem. Soc. 131 (2009) 3985–3990.
[35] C.-H. Chang, Y.-L. Lee, Appl. Phys. Lett. 91 (2007) 053503.
[36] Y. Lai, Z. Lin, D. Zheng, L. Chi, R. Du, C. Lin, Electrochim. Acta 79 (2012) 175–181.
[37] V. Chakrapani, D. Baker, P.V. Kamat, J. Am. Chem. Soc. 133 (2011) 9607–9615.
[38] Y.-L. Lee, C.-H. Chang, J. Power Sources 185 (2008) 584–588.
[39] E. Hosono, S. Fujihara, K. Kakiuchi, H. Imai, J. Am. Chem. Soc. 126 (2004) 7790–7791.
[40] K. Kakiuchi, E. Hosono, H. Imai, T. Kimura, S. Fujihara, J. Cryst. Growth 293 (2006) 541–545.
[41] Z.-J. Zhou, J.-Q. Fan, X. Wang, W.-H. Zhou, Z.-L. Du, S.-X. Wu, ACS Appl. Mater. Interfaces 3 (2011) 4349–4353.
[42] U. Diebold, Appl. Phys. A Mater. Sci. Process. 76 (2003) 681–687.
[43] M. Gao, Y. Li, M. Guo, M. Zhang, X. Wang, J. Mater. Sci. Technol. 28 (2012) 577–586.
[44] M. Xu, P. Da, H. Wu, D. Zhao, G. Zheng, Nano Lett. 12 (2012) 1503–1508.
[45] W.W. Yu, L. Qu, W. Guo, X. Peng, Chem. Mater. 15 (2003) 2854–2860.
[46] Y.-L. Lee, Y.-S. Lo, Adv. Funct. Mater. 19 (2009) 604–609.
[47] S.W. Jung, J.-H. Kim, H. Kim, C.-J. Choi, K.-S. Ahn, J. Appl. Phys. 110 (2011) 044313.
[48] Y.-L. Lee, C.-F. Chi, S.-Y. Liau, Chem. Mater. 22 (2010) 922–927.
[49] A. Zaban, M. Greenshtein, J. Bisquert, ChemPhysChem 4 (2003) 859–864.
[50] T. Zeng, H. Tao, X. Sui, X. Zhou, X. Zhao, Chem. Phys. Lett. 508 (2011) 130–133.
[51] I. Robel, M. Kuno, P.V. Kamat, J. Am. Chem. Soc. 129 (2007) 4136–4137.
[52] J.G. Radich, R. Dwyer, P.V. Kamat, J. Phys. Chem. Lett. 2 (2011) 2453–2460.
[53] S.W. Jung, J.-H. Kim, H. Kim, C.-J. Choi, K.-S. Ahn, Curr. Appl. Phys. 12 (2012) 1459–1464.
[54] S.S. Kalanur, S.Y. Chae, O.S. Joo, Electrochim. Acta 103 (2013) 91–95.